Letter

An Electrochemical Sensor Based on Chalcogenide Molybdenum Disulfide-Gold-Silver Nanocomposite for Detection of Hydrogen Peroxide Released by Cancer Cells

Jinchun Hu [†], Congcong Zhang [†], Xue Li and Xin Du *

Shandong Provincial Key Laboratory of Animal Resistance Biology, Key Laboratory of Food Nutrition and Safety, College of Life Sciences, Shandong Normal University, Jinan 250014, China; hujinchun_369@163.com (J.H.); zhangcc1026@163.com (C.Z.); lx1213940737@163.com (X.L.)

* Correspondence: xdu@sdnu.edu.cn; Tel.: +86-136-5640-1019

† These authors contributed equally to this work.

check for updates

Abstract: Hydrogen peroxide (H_2O_2) as a crucial signal molecule plays a vital part in the growth and development of various cells under normal physiological conditions. The development of H_2O_2 sensors has received great research interest because of the importance of H_2O_2 in biological systems and its practical applications in other fields. In this study, a H_2O_2 electrochemical sensor was constructed based on chalcogenide molybdenum disulfide–gold–silver nanocomposite (MoS_2-Au-Ag). Transmission electron microscopy (TEM), X-ray photoelectron spectroscopy (XPS) and energy dispersive spectroscopy (EDS) were utilized to characterize the nanocomposites, and the electrochemical performances of the obtained sensor were assessed by two electrochemical detection methods: cyclic voltammetry and chronoamperometry. The results showed that the MoS_2-Au-Ag-modified glassy carbon electrode (GCE) has higher sensitivity (405.24 μA mM^{-1} cm^{-2}), wider linear detection range (0.05–20 mM) and satisfactory repeatability and stability. Moreover, the prepared sensor was able to detect the H_2O_2 discharge from living tumor cells. Therefore, this study offers a platform for the early diagnosis of cancer and other applications in the fields of biology and biomedicine.

Keywords: hydrogen peroxide; tumor cells; molybdenum disulfide–gold–silver; electrochemical sensor; detection

1. Introduction

Cells can produce all kinds of reactive oxygen species in metabolic process, and H_2O_2 is one of the most momentous representatives. H_2O_2 plays a vital role in numerous processes such as cellular signal transduction, apoptosis and many other physiological processes [1]; however, excess H_2O_2 is toxic to humans, which leads to various diseases, such as cancer, cardiovascular disease and neurodegenerative diseases [2]. Research has proved that cancer cells will release excessive H_2O_2 to achieve the abnormal growth of tumors. Therefore, the accurate and fast determination of H_2O_2 is significant in the cellular environment and diagnosing cancer in its early stages. Additionally, H_2O_2 is widely used as an oxidizer, disinfectant or bleach in the food, environmental analysis, chemical and pharmaceutical industries [3,4].

The traditional methods for the detection of H_2O_2 include spectrophotometry [5], chemiluminescence [6,7], fluorescence [8,9] and high performance liquid chromatography [10]. However, these methods also have some limitations, such as expensive equipment and cumbersome

procedures. Electrochemical detection is a detective method which has the advantages of high sensitivity, low cost, high efficiency and good portability [11]. In recent years, the development of nanomaterials has provided many new opportunities for the construction of hydrogen peroxide sensors. Nanomaterials have the unique properties of a strong adsorption capacity, large specific surface area and high catalytic efficiency [12,13]. In the field of electrochemical sensors, the application of nanomaterials not only improves the stability and sensitivity of electrodes, but also improves the detection performance of sensors [13].

MoS_2 has attracted extensive attention in the studies of lithium batteries, catalysts and cancer treatment owing to its advantages of good stability, high catalytic efficiency and easy functionalization [14–16]. The structure of single-layer MoS_2 is composed of two layers of sulfur sandwiched by a layer of molybdenum. The atoms are covalently bonded to each other, which shows as a sandwich structure [17]. At present, the sensors using molybdenum disulfide as the experimental material are involved in the detection of glucose, hydrogen peroxide, nucleic acid, protein and other substances which showed a good sensitivity and detection performance. Au, Ag and other precious metal nanomaterials not only have the characteristics of general nanometer materials, but also have excellent electrical conductivity, a unique catalytic activity and are non-toxic, which makes them have unique advantages and extensive applications in the field of sensors [18,19].

Herein, we developed a sensitive sensor for the detection of H_2O_2 discharge from tumor cells by using a MoS_2-Au-Ag nanocomposite to accomplish high conductivity and increase the surface area of the electrode, due to the fact that H_2O_2 is a typical tumor biomarker and the developed MoS_2-Au-Ag electrode exhibits an excellent enzyme-mimic electrocatalytic activity in the oxidation of H_2O_2. We chose cyclic voltammetry (CV) to evaluate the properties of our fabricated sensor for the detection of H_2O_2, which is a very sensitive electrochemical detection tool used to evaluate the performance of an electrochemical sensor [19]. Our results indicated that this sensor significantly improved the detection signal and consequently enhanced the low detection limit with a wide detection range, and high selectivity and sensitivity. This study demonstrates a functional, non-enzymatic electrochemical sensor based on MoS_2-Au-Ag nanocomposite for the detection of H_2O_2 released by normal and tumor cells.

2. Experimental

2.1. Chemicals and Reagents

MoS_2, phthalic diglycol diacrylate (PDDA), $K_3[Fe(CN)_6]$, phorbol 12-myristate 13-acetate (PMA), chloroauric acid ($H[AuCl_4]$) and $AgNO_3$ were obtained from Sigma (USA). H_2O_2 was purchased from Shanghai Wokai Biotechnology Co., Ltd. (China). C_2H_5OH was obtained from Tianjin Chemical Reagent Sixth Factory (China). KCl was purchased from Shanghai Hutan Laboratory Equipment Co., Ltd. (China). Phosphate buffer solution (PBS) was obtained from Biological Industries. 3-(4,5-dimethylthiazol-2-yl)-2,5-diphenyltetrazolium bromide (MTT) was obtained from Beijing Solarbio Science & Technology Co., Ltd. (China). The RPE-1 human retinal pigment epithelial cell line and the MCF-7 human breast cancer cell line were purchased from the cell bank of the Chinese Academy of Sciences (Shanghai, China). For the configuration of all aqueous solutions and to clean all materials we used twofold distilled water.

2.2. Electrochemical Measurements

The electrochemical detection used a standard three-electrode electrochemical testing device with a glassy carbon electrode modified by nanomaterials as the working electrode, and a silver/silver chloride (Ag/AgCl) and platinum wire were used as the reference electrode and counter electrode, respectively. The electrochemical test was conducted in PBS or cell samples, which were deoxygenated with N_2 and stirred with a magnetic agitator at a speed of 300 rpm to maintain a stable and uniform H_2O_2 concentration in the solution.

2.3. Dispersion of MoS$_2$

The dispersing agent PDDA was used to disperse the MoS$_2$ into a uniform and stable dispersion by taking 3 mg and 7.5 mg MoS$_2$ into a 1.5 mL centrifuge tube and then adding 1% or 0.5% PDDA at a constant volume to 1.5 mL. Next, we got a MoS$_2$ solid precipitate via sonication for 2 h and centrifuged it at 15,000 rpm for 10 min. Subsequently, four different concentrations of dispersion were obtained by discarding the supernatant and adding water at a constant volume to 1.5 mL, including 2 mg mL^{-1} and 5 mg mL^{-1} MoS$_2$ dispersions with 0.5% and 1% PDDA.

2.4. Preparation of MoS$_2$-Au-Ag/GCE

The bare GCE was pre-polished with 0.3 μm and 0.05 μm alumina powders to get a smooth mirror surface before fabricating with a modified electrode [20]. For the purpose of wiping off the physically adsorbed substance, GCE was then sonicated with the mixture solution of ultra-pure water and ethanol for 10 min. After that, the cleaned electrode was dried under N$_2$. Briefly, 10 μL of MoS$_2$ suspension (2 mg mL^{-1}) was cautiously dropped onto the GCE surface, and the modified electrode was dried under air. Then, MoS$_2$/GCE was electrodeposited in 2.5 mM H[AuCl$_4$] and 2.5 mM AgNO$_3$ solutions, respectively, under the condition of −0.4 V. Accordingly, the MoS$_2$-Au-Ag/GCE was successfully prepared. The whole process of the fabrication is illustrated in Scheme 1.
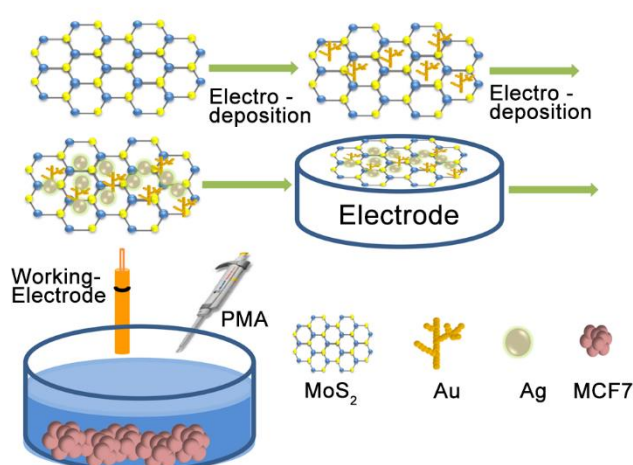
Scheme 1. Fabrication and detection of the H$_2$O$_2$ electrochemical sensor.

2.5. Detection of H$_2$O$_2$ Solutions with Different Concentrations and Released by Cells

The 30% pure H$_2$O$_2$ solution was diluted into 100 mM, 400 mM, 2000 mM and 4000 mM H$_2$O$_2$ with PBS, and the corresponding concentration of H$_2$O$_2$ was added to the 20 mL PBS buffer liquid system to conduct electrochemical detection of the modified electrodes. RPE-1 cells and MCF-7 cells were cultured in DMEM medium containing 10% fetal bovine serum (FBS), and were grown in a cell culture incubator with 5% CO$_2$ and 37 °C. After they were grown to 80–90% confluence, the cells were washed 2–3 times with PBS, and resuspended into 2 mL oxygen-removing PBS for electrochemical detection of H$_2$O$_2$ generated by the MCF-7 cells. With the cell-free group as the control group and three groups of cells with different concentrations as the experimental group, the flux of H$_2$O$_2$ caused by normal cells and living cancer cells upon the addition of PMA at different concentrations and the correlated electrochemical response signals were recorded by amperometric i-t curves. The effect of the nanomaterials in the cell culture was assessed via an MTT assay and the detailed experimental steps can be found in Supporting Information.

3. Results and Discussion

3.1. Characterization of MoS$_2$-Au-Ag/GCE Nanocomposite

The morphology and structure of the obtained nanomaterials were investigated by TEM. Figure 1A shows that the MoS$_2$ has a uniform lamellar structure. As illustrated in Figure 1B,C, the Au and Ag nanoparticles showed clear dendritic and granular morphologies, respectively, and were evenly dispersed over the MoS$_2$. As shown in Figure 1D, the MoS$_2$-Au-Ag mimics uniformly compact branches in the PDDA solution. In summary, we successfully synthesized the MoS$_2$-Au-Ag nanocomposite, which has potential application value for improving electrochemical detection performance. The chemical composition of MoS$_2$-Au-Ag was verified by XPS. As shown in Figure S1, the curve presented O 1s peaks, C 1s peaks, Ag 3d peaks, Mo 3d peaks, Au 4f peaks and S 2p peaks in one spectrum. For the Mo 3d region, the two characteristic peaks at 229.8 eV and 233.5 eV corresponded to Mo 3d$_{5/2}$ and Mo 3d$_{3/2}$ of MoS$_2$, respectively, and the single S 2s peak is located at about 227 eV. Meanwhile, the binding energies at 162.1 eV and 163.2 eV can be attributed to the S 2p$_{3/2}$ and S 2p$_{1/2}$ species on the edges or surface of the MoS$_2$ nanosheet, respectively. In addition, the strong peaks of the elements Au and Ag confirmed the successful electrodeposition of two metals on the glassy carbon electrode modified with MoS$_2$. In addition, energy dispersive spectroscopy (EDS) was used to analyze and study the components of the MoS$_2$-Au-Ag. The element of Mo, S, Au and Ag were clearly observed, which originated from the MoS$_2$, Au and Ag nanomaterials, respectively (Figure 1E). The results further manifested that MoS$_2$-Au-Ag was constructed successfully. We also studied the effects of different materials on sensor performance (Figure 2). The resulting spectra manifested that the oxidation and reduction peaks associated with MoS$_2$-Au/GCE (b) and MoS$_2$-Au-Ag/GCE (c) increased substantially compared with MoS$_2$/GCE (a). Moreover, the peak value of redox was the largest for MoS$_2$-Au-Ag/GCE, demonstrating that the Au-Ag nanocomposite particles have a good effect on enhancing electrode conductivity. The MoS$_2$-Au-Ag composite was used to modify the electrode in the subsequent experiments.
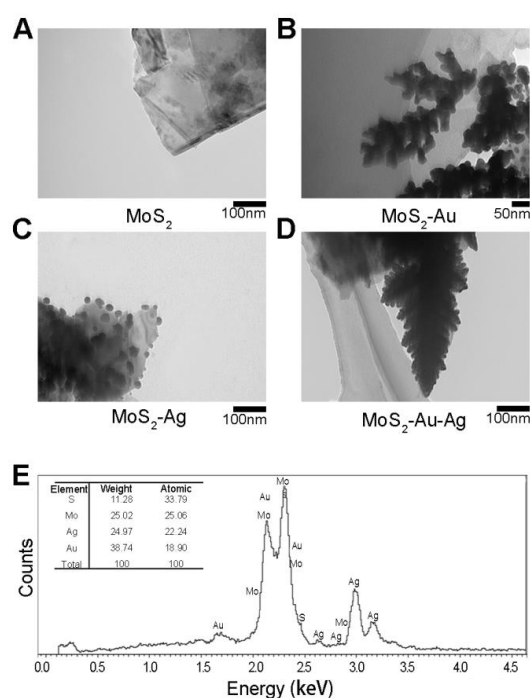

Figure 1. Characterization of the morphology, structure, and electrochemical performance of the nanocomposites. (**A–D**) Transmission electron microscopy images of MoS$_2$ (**A**), MoS$_2$-Au (**B**), MoS$_2$-Ag (**C**) and MoS$_2$-Au-Ag (**D**). (**E**) The X-ray energy dispersive spectrometric analysis of MoS$_2$-Au-Ag.
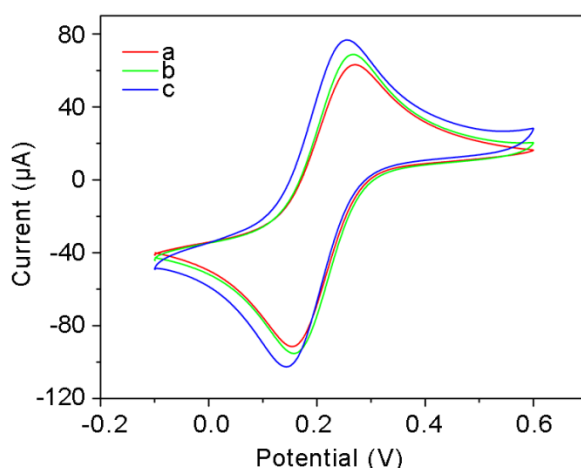
Figure 2. Cyclic voltammetry of nanomaterials. CV profiles of MoS$_2$/GCE (a), MoS$_2$-Au/GCE (b), MoS$_2$-Au-Ag/GCE (c) recorded in K$_3$[Fe(CN)$_6$].

3.2. Optimization of Experimental Parameters for the Fabrication of MoS$_2$-Au-Ag/GCE

Changes in the experimental conditions of the modified electrode will directly affect the electrochemical properties of the electrode, which will lead to alterations of the catalytic properties and sensor functions [21]. For the sake of enhancing the sensing performance of the MoS$_2$-Au-Ag/GCE, the effects of the PDDA concentration of dispersed MoS$_2$, the electrodeposition time, and the modified electrode material were investigated.

MoS$_2$ was dispersed with water, PBS buffer and PDDA of different concentrations, and then placed in a 4 °C refrigerator for 4 h after ultrasound to observe the dispersion (Figure 3A). The results showed that the MoS$_2$ dispersed with water and PBS buffer had obvious precipitation and was not dissolved at all. The dispersion of MoS$_2$ with PDDA was better, and a uniform MoS$_2$ dispersion was obtained. The effect of PDDA concentration on the electrochemical property of MoS$_2$-Au-Ag/GCE was analyzed by CV in K$_3$[Fe(CN)$_6$]. As shown in Figure 3B, the peak current values of 2 mg mL^{-1} MoS$_2$ with 1% PDDA (b) and 5 mg mL^{-1} MoS$_2$ with 1% PDDA (c) are similar. Based on the principle of economy, 2 mg mL^{-1} MoS$_2$ with 1% PDDA was selected for subsequent experiments. The Au-Ag electrodeposited on the surface of MoS$_2$/GCE can provide a large effective surface area and enhance the electrocatalytic performance of the electrode, which is of great significance for the determination of H$_2$O$_2$ [22]. Thus, the amount of Au-Ag electrodeposited on the surface of MoS$_2$/GCE immediately affects the performance of the H$_2$O$_2$ sensor. To enhance the function of Au-Ag on the MoS$_2$/GCE, the effect of electrodeposition time from 30 s to 150 s was analyzed by CV in 10 mM H$_2$O$_2$, as shown in Figure 3D. The analysis results revealed that the potential and the current value of redox peak were different. As we can see from Figure 3C, the b and d peak current values are bigger, but the peak potential value of b is larger. As such, we chose the optimized electrodeposition time in the fabrication of modified electrode to reduce the interference of high voltage.

3.3. Electrocatalytic Activities of the Modified Electrodes

We employed CV to research the electrocatalytic activities of MoS$_2$/GCE, MoS$_2$-Au/GCE and MoS$_2$-Au-Ag/GCE in 5 mM H$_2$O$_2$ (Figure 4A). The CV experiments revealed that no redox peaks were measured relating to MoS$_2$/GCE (a) in the range of −0.80 V–0.00 V, while MoS$_2$-Au/GCE (c) and MoS$_2$-Au-Ag/GCE (d) had the presence of a reduction peak of H$_2$O$_2$ at −0.50 V. Therefore, MoS$_2$-Au-Ag/GCE had a better reaction performance to H$_2$O$_2$.
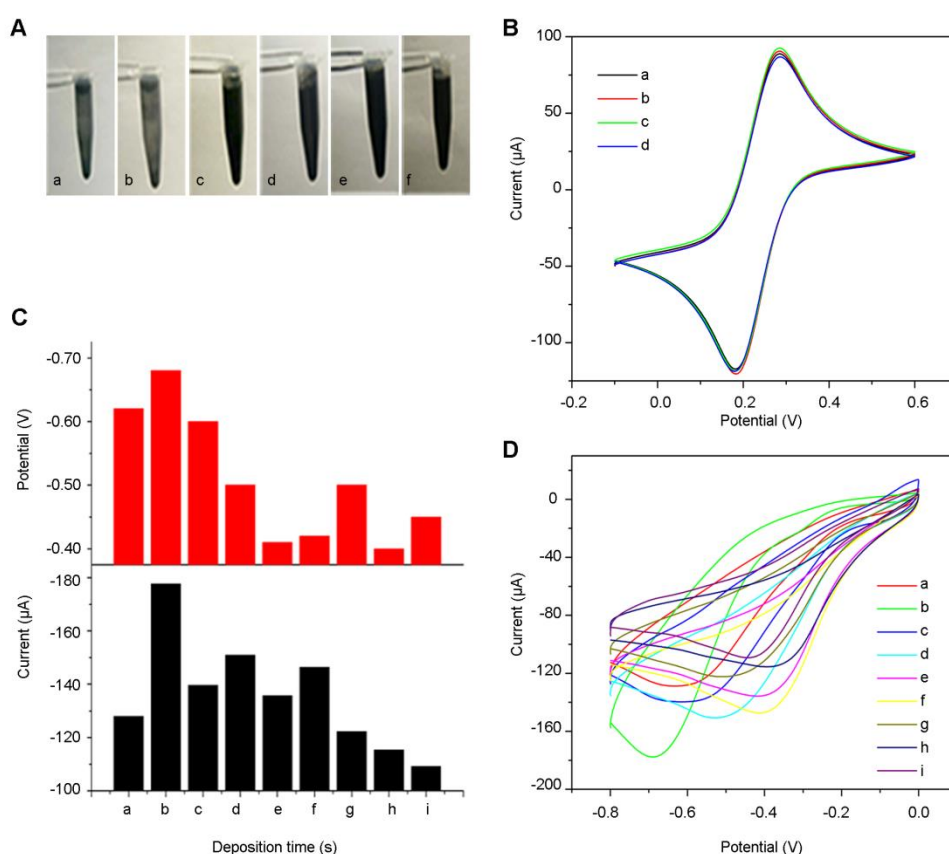
Figure 3. Optimization of experimental parameters for the fabrication of MoS$_2$-Au-Ag/GCE. (**A**) MoS$_2$ dispersion effects of 2 mg mL^{-1} water (a), 2 mg mL^{-1} PBS buffer (b), 5 mg mL^{-1} 0.5% PDDA (c), 5 mg mL^{-1} 1% PDDA (d), 2 mg mL^{-1} 0.5% PDDA (e) and 2 mg mL^{-1} 1% PDDA (f). (**B**) CV curves of dispersed MoS$_2$ modified electrodes in K$_3$[Fe(CN)$_6$] under 2 mg mL^{-1} 0.5% PDDA (a), 2 mg mL^{-1} 1% PDDA (b), 5 mg mL^{-1} 1% PDDA (c), 5 mg mL^{-1} 0.5% PDDA (d). (**C**) The current line diagram of the electrode at 10 mM H$_2$O$_2$ with different deposition times. (**D**) CV curves of electrode modified with different depositions time in 10 mM H$_2$O$_2$. Deposition time: (a) Au 30 s Ag 30 s, (b) Au 30 s Ag 90 s, (c) Au 30 s Ag 150 s, (d) Au 90 s Ag 30 s, (e) Au 90 s Ag 90 s, (f) Au 90 s Ag150 s, (g) Au 150 s Ag 30 s, (h) Au 150 s Ag 90 s, (i) Au 150 s Ag 150 s.

We then examined the CV results of MoS$_2$-Au-Ag/GCE in PBS and in different concentrations of H$_2$O$_2$ (Figure 4B). The redox peak of modified electrodes was not measured in PBS (a) while it was shown in 5 mM (b) and 10 mM H$_2$O$_2$ (c). With the increase in concentration of H$_2$O$_2$, the reductive peak position shifting to the left may be due to the delay of electron transfer caused by the increase in H$_2$O$_2$ concentration. In order to prevent interference from other substances, −0.45 V was selected as the catalytical voltage for subsequent current response experiments. Compared with the 5 mM H$_2$O$_2$ solution, the reduction peak current value measured by the modified electrode in 10 mM H$_2$O$_2$ increased significantly, indicating that MoS$_2$-Au-Ag/GCE had a higher sensitivity to H$_2$O$_2$.

The kinetics of the MoS$_2$-Au-Ag/GCE were investigated by analyzing the impacts of the scan rate on the redox current. The electrochemical performance of MoS$_2$-Au-Ag/GCE was examined in 10 mM K$_3$[Fe(CN)$_6$] with the increase of scan rate from 10 to 100 mV s^{-1}. As displayed in Figure 4C, a great linear relationship was shown between the square root of scan rate and the peak current density. The maximum current of the redox peak was increased linearly and the distance of the peak was expanded gradually. According to these results, we made a linear fit of the oxidation peak (I_{pa}) and reduction (I_{pc}) peak currents with the square root of the scan rate ($v^{1/2}$). The relevant linear regression equations were $I_{pa} = 14.89\ v^{1/2} - 13.74$ and $I_{pc} = -15.37\ v^{1/2} - 15.26$ with correlation coefficients of 0.9916

and 0.9976, respectively (Figure 4D). The electrochemical signal of the modified electrode suggests that the catalysis process is diffusion controlled.
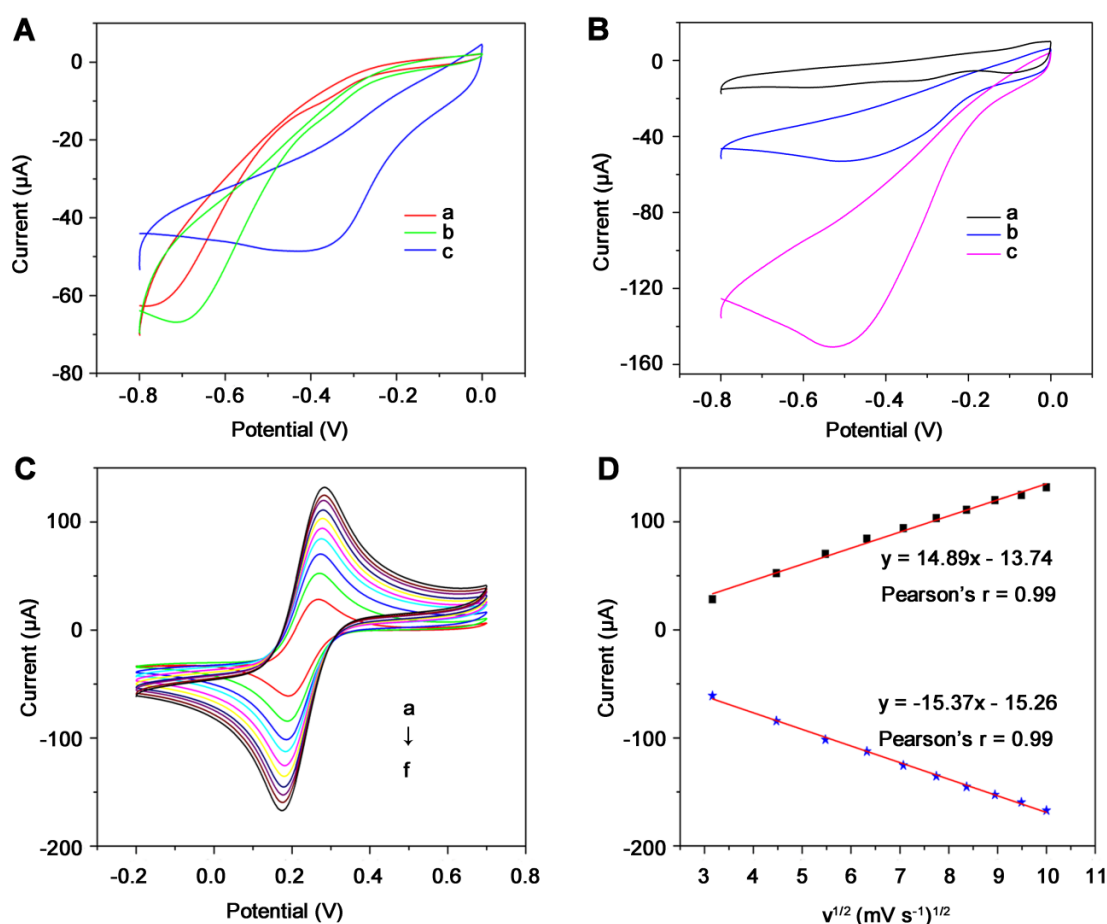

Figure 4. Electrocatalytic activities of the modified electrodes. (**A**) CV profiles of electrode modified by MoS_2/GCE (a), MoS_2-Au/GCE (b) and MoS_2-Au-Ag/GCE (c) in 5 mM H_2O_2. (**B**) CV curves of MoS_2-Au-Ag/GCE in PBS (a), 5 mM H_2O_2 (b) and 10 mM H_2O_2 (c). (**C**) Kinetic analysis of MoS_2-Au-Ag/GCE at scan rates ranging from 10 to 100 mV s^{-1}. (**D**) Linear fits of the oxidized peak current (I_{pa}) and reduced peak current (I_{pc}) versus the square root of the scan rate ($v^{1/2}$).

3.4. Amperometric Responses to H_2O_2

To further detect the amperometric current responses of MoS_2-Au-Ag/GCE, we added H_2O_2 at different concentrations continuously at a potential of −0.45 V. To prevent interference, H_2O_2 was added for the first time after the current was kept at a stable value, and then added every 50 s. Figure 5A shows the amperometric response of MoS_2-Au-Ag/GCE with various concentrations of H_2O_2. After injecting a certain amount of H_2O_2, MoS_2-Au-Ag/GCE exhibited a fast current response because of the excellent electrocatalytic performance of MoS_2-Au-Ag. It can be clearly seen that each reduction current response demonstrated an explicit increase as the concentration of H_2O_2 increased and the response current attained a steady state within 4 s. The illustration manifests the amperometric current response at lower concentrations of H_2O_2 (0.05 mM–0.75 mM).
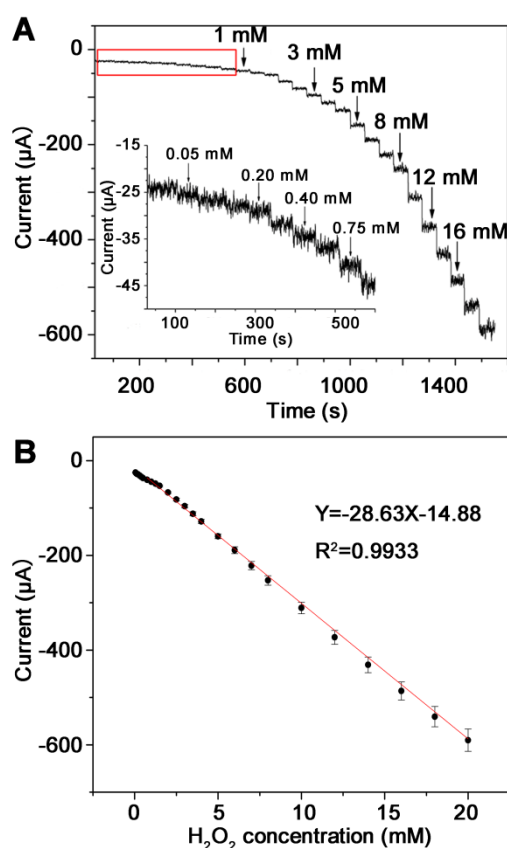
Figure 5. Kinetics of MoS_2-Au-Ag/GCE. (**A**) The i-t curve of the MoS_2-Au-Ag/GCE when different concentrations of H_2O_2 were added to the PBS buffer successively. (**B**) Linear fitting diagram.

As shown in Figure 5B, the calibration curve was fitted by using multiple sets of repeated experimental data. According to the curve fitting, we calculated the linear range of the prepared sensor to be from 0.05 mM to 20 mM, with a linear correlation coefficient of 0.9933, and the sensitivity was 405.24 $\mu A\ mM^{-1}\ cm^{-2}$ (28.63 $\mu A\ mM^{-1}$). It is worth noting that the sensitivity is much higher than many reported H_2O_2 sensors, as shown in Table 1. The detection equation of the sensor was Y = −28.63 X − 14.88 and the minimum detection limit was 7.19 μM. This experiment further demonstrated that the MoS_2-Au-Ag composite is an excellent material for H_2O_2 detection with good sensitivity.

Table 1. Comparison of the performances of various H_2O_2 sensors.

Material	Sensitivity ($\mu A\ mM^{-1}\ cm^{-2}$)	Detection Limit (μM)	Linear Range (mM)	Reference
Pt/OMCs	184.6	1.2	0.5–4.5	[23]
Ag-TiO_2	65.23	0.83	0.0083–0.0433	[24]
ZIF-67/CNFs	323	0.62	0.0025–0.19	[25]
Pt-SnO_2@C	241.1	0.1	0.001–0.17	[26]
PANI/HRP/SWCNTs	200	900	2.5–50	[27]
MoS_2-Au-Ag	405.24	7.19	0.05–20	this work

3.5. Repeatability and Stability of MoS$_2$-Au-Ag/GCE

The repeatability and stability of the electrochemical sensor are the main parameters affecting the applicability of the H_2O_2 sensor. The current response values of five modified electrodes when 1 mM H_2O_2 was successively injected under the same conditions are recorded in Figure 6A. The RSD of the relative standard deviation of the five electrodes was calculated to be 3.79%. The stability was evaluated

by placing the MoS$_2$-Au-Ag/GCE in PBS buffer and adding 1 mM H$_2$O$_2$ continuously (Figure 6B). The modified electrode was tested every 4 h and then placed overnight in a 4 °C refrigerator for further testing. The response current of the i-t curve detected for the first time at a large concentration has some deviation from other curves, but the deviation is small, and the other curves almost coincide, yielding an RSD of 3.09%. Thus, the MoS$_2$-Au-Ag electrode shows a good repeatability and an acceptable stability, indicating that the MoS$_2$-Au-Ag composite material has a good application prospect in H$_2$O$_2$ detection.
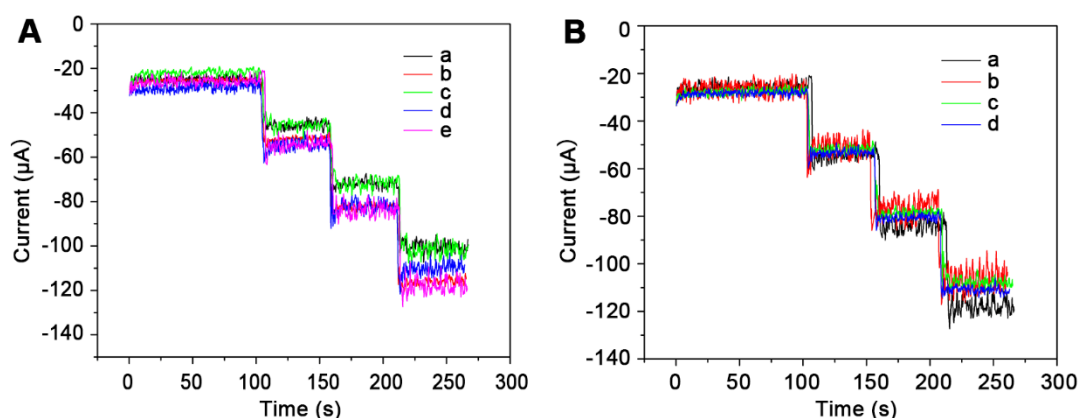
Figure 6. Results obtained using the H$_2$O$_2$ sensor are highly sensitive and reproducible. (**A**) The i-t curves of MoS$_2$-Au-Ag/GCE were dripped with the same concentration of H$_2$O$_2$ into PBS. (**B**) The i-t curves of the same MoS$_2$-Au-Ag/GCE when the same concentration of H$_2$O$_2$ was dripped into PBS after the electrode was placed at different times.

3.6. Detection of H$_2$O$_2$ Released from Normal Cells and Living Cancer Cells

H$_2$O$_2$ is an important representative of the reactive oxygen species related to lots of cellular life activities, and is a potential biomarker for cancer cells [28–30]. In order to better explore the physiological processes of early-stage cancer cells, the monitoring of H$_2$O$_2$ levels in the cell environment is crucial. In this study, we selected human breast cancer cells (MCF-7) for the on-site real-time monitoring of H$_2$O$_2$ release after stimulation. First, an MTT assay was used to evaluate the effects of the prepared nanomaterials on living cancer cells. The results showed that the survival rate of these living tumor cells all reached more than 90% after 24 h of co-incubation, even with 25 µg mL^{-1} nanomaterials, so the cell growth was almost unchanged and the original activity was maintained (Figure 7D). Therefore, it can be proven that the MoS$_2$-Au-Ag nanocomposite was biocompatible with living cells and can be used for further electrochemical tests. Moreover, the dynamic release of H$_2$O$_2$ by pure a PBS solution and MCF-7 cells of different concentrations was detected using the MoS$_2$-Au-Ag sensor before and after the stimulation of PMA. As depicted in Figure 7A, we observed a significantly reduced current increase upon the addition of 40 µL PMA (0.5 mg mL^{-1}) when the PBS was suspended with MCF-7 cells. The control group with the absence of MCF-7 cells (a) showed no detectable current response to the injection of PMA, indicating that the triggered H$_2$O$_2$ was the result of PMA-stimulated cells. In addition, curves b, c, and d showed the current response curve of the MoS$_2$-Au-Ag sensor at –0.4 V in the presence of the 10%, 30% and 50% concentrations of MCF-7 cells by physiological injection of PMA, respectively. The results revealed that the reduction current increases more significantly as the cell concentration increases. Besides, hydrogen peroxide, released by human retinal pigment epithelial cells (RPE-1), was detected under the same conditions. As shown in Figure 7B, we observed that the control group (a) without RPE-1 cells showed no current response after PMA injection, while the experimental group with PMA stimulation showed a slight decrease in current. Compared with the MCF-7 cells, RPE-1 cells showed a very weak reduction in response current, further indicating that the triggered H$_2$O$_2$ was the result of the stimulation of cancer cells by PMA, as exhibited in Figure 7C.

In conclusion, the proposed MoS$_2$-Au-Ag sensor could be utilized to detect the H$_2$O$_2$ released by living cancer cells, and it has the potential to be used as a physiological and pathological H$_2$O$_2$ sensor for the diagnosis and treatment of cancer in its early stages.
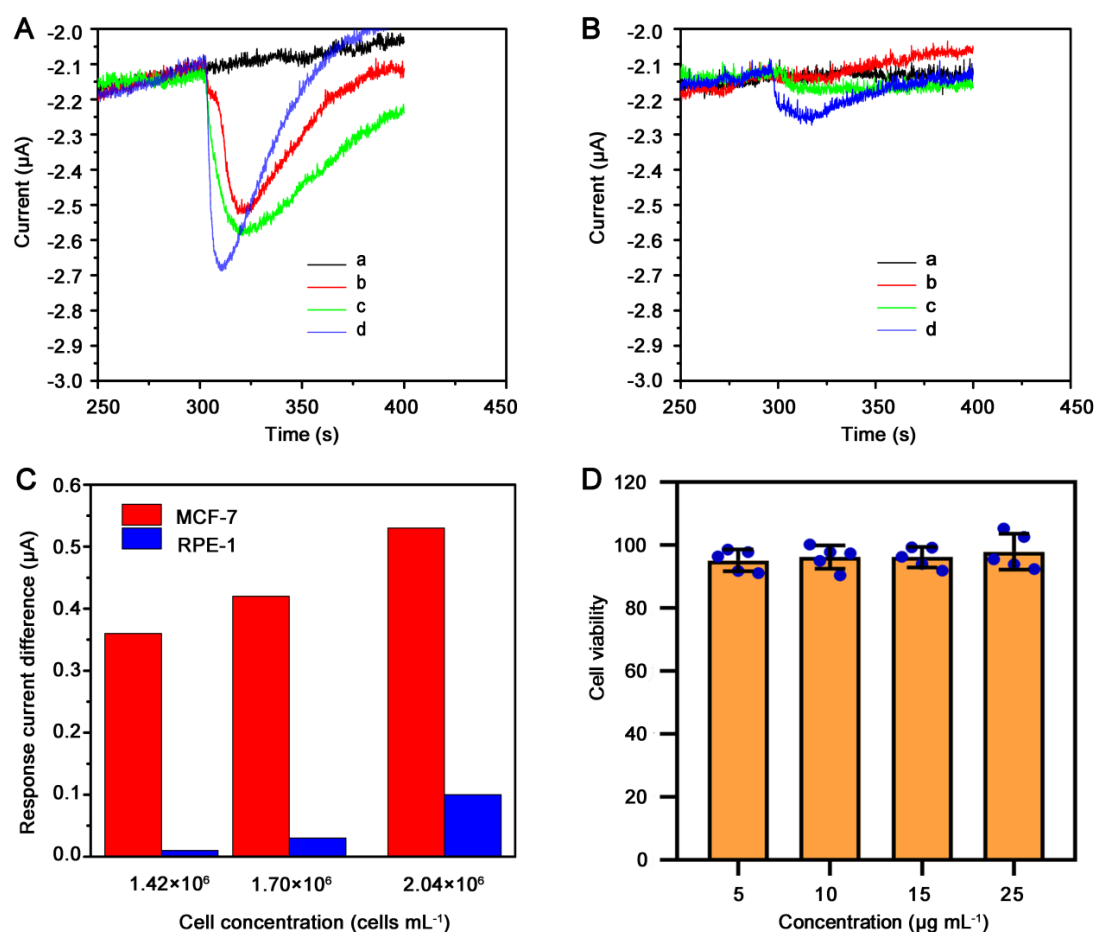

Figure 7. Detection of H$_2$O$_2$ released from normal cells and living cancer cells. (**A**) Amperometric response of MoS$_2$-Au-Ag/GCE to injection of 200 ng mL^{-1} PMA with MCF-7 cells in 0.1 M PBS (pH 7.4). (**B**) Amperometric response of MoS$_2$-Au-Ag/GCE to injection of 200 ng mL^{-1} PMA with RPE-1 cells in 0.1 M PBS (pH 7.4). (**C**) Comparison of response current differences between MCF-7 and RPE-1 cells induced by H$_2$O$_2$ release. (**D**) Effects of prepared MoS$_2$-Au-Ag on metabolic activities of MCF-7 cells.

4. Conclusions

In summary, we constructed an H$_2$O$_2$ sensor based on MoS$_2$-Au-Ag nanocomposites by electrodepositing Au and Ag nanoparticles to modify MoS$_2$/GCE. The resulting MoS$_2$-Au-Ag/GCE exhibited an excellent electrochemical performance with a sensitivity of 405.24 μA mM^{-1} cm^{-2} (28.63 μA mM^{-1}) and a linear detection range of 0.05 mM to 20 mM. The H$_2$O$_2$ sensor has good repeatability and stability, and a short response time. The H$_2$O$_2$ sensor constructed in this study has also been successfully applied in the detection of H$_2$O$_2$ generated by living cancer cells, indicating that this work is expected to play a significant role in the early diagnosis and treatment of tumors and providing an important basis for the development of effective treatment strategies. Thus, we believe that the prepared MoS$_2$-Au-Ag sensor can be used to analyze H$_2$O$_2$ in all sorts of samples, and we can continue to miniaturize it for better clinical testing in the future.

References

1. Juang, F.-R.; Chern, W.-C. Octahedral Cu$_2$O nanoparticles decorated by silver catalyst for high sensitivity nonenzymatic H$_2$O$_2$ detection. *Mater. Sci. Semicond. Process.* **2019**, *101*, 156–163. [CrossRef]

2. Ohshima, H.; Tatemichi, M.; Sawa, T. Chemical basis of inflammation-induced carcinogenesis. *Arch. Biochem. Biophys.* **2003**, *417*, 3–11. [CrossRef]

3. Ye, Y.; Kong, T.; Yu, X.; Wu, Y.; Zhang, K.; Wang, X. Enhanced nonenzymatic hydrogen peroxide sensing with reduced graphene oxide/ferroferric oxide nanocomposites. *Talanta* **2012**, *89*, 417–421. [CrossRef]

4. Lu, N.; Zhang, T.; Yan, X.; Gu, Y.; Liu, H.; Xu, Z.; Xu, H.; Li, X.; Zhang, Z.; Yang, M. Facile synthesis of 3D N-doped porous carbon nanosheets as highly active electrocatalysts toward the reduction of hydrogen peroxide. *Nanoscale* **2018**, *10*, 14923–14930. [CrossRef]

5. Zou, J.; Cai, H.H.; Wang, D.Y.; Xiao, J.Y.; Zhou, Z.M.; Yuan, B.L. Spectrophotometric determination of trace hydrogen peroxide via the oxidative coloration of DPD using a Fenton system. *Chemosphere* **2019**, *224*, 646–652. [CrossRef]

6. Yuan, J.C.; Shiller, A.M. Determination of subnanomolar levels of hydrogen peroxide in seawater by reagent-injection chemiluminescence detection. *Anal. Chem.* **1999**, *71*, 1975–1980. [CrossRef]

7. Yang, X.J.; Li, R.S.; Li, C.M.; Li, Y.F.; Huang, C.Z. Cobalt oxyhydroxide nanoflakes with oxidase-mimicking activity induced chemiluminescence of luminol for glutathione detection. *Talanta* **2020**, *215*. [CrossRef]

8. Han, H.; He, X.; Wu, M.X.; Huang, Y.B.; Zhao, L.H.; Xu, L.L.; Ma, P.Y.; Sun, Y.; Song, D.Q.; Wang, X.H. A novel colorimetric and near-infrared fluorescence probe for detecting and imaging exogenous and endogenous hydrogen peroxide in living cells. *Talanta* **2020**, *217*. [CrossRef]

9. Ren, M.G.; Deng, B.B.; Wang, J.Y.; Kong, X.Q.; Liu, Z.R.; Zhou, K.; He, L.W.; Lin, W.Y. A fast responsive two-photon fluorescent probe for imaging H$_2$O$_2$ in lysosomes with a large turn-on fluorescence signal. *Biosens. Bioelectron.* **2016**, *79*, 237–243. [CrossRef]

10. Wen, Y.; Liu, K.; Yang, H.; Li, Y.; Lan, H.; Liu, Y.; Zhang, X.; Yi, T. A highly sensitive ratiometric fluorescent probe for the detection of cytoplasmic and nuclear hydrogen peroxide. *Anal. Chem.* **2014**, *86*, 9970–9976. [CrossRef]

11. Diouf, A.; El Bari, N.; Bouchikhi, B. A novel electrochemical sensor based on ion imprinted polymer and gold nanomaterials for nitrite ion analysis in exhaled breath condensate. *Talanta* **2020**, *209*, 120577. [CrossRef] [PubMed]

12. Aragay, G.; Merkoci, A. Nanomaterials application in electrochemical detection of heavy metals. *Electrochim. Acta* **2012**, *84*, 49–61. [CrossRef]

13. Liu, M.; Xie, S.B.; Zhou, J. Use of animal models for the imaging and quantification of angiogenesis. *Exp. Anim.* **2018**, *67*, 1–6. [CrossRef] [PubMed]

14. Akter, R.; Rahman, M.A.; Rhee, C.K. Amplified electrochemical detection of a cancer biomarker by enhanced precipitation using horseradish peroxidase attached on carbon nanotubes. *Anal. Chem.* **2012**, *84*, 6407–6415. [CrossRef]

15. Kibsgaard, J.; Chen, Z.; Reinecke, B.N.; Jaramillo, T.F. Engineering the surface structure of MoS$_2$ to preferentially expose active edge sites for electrocatalysis. *Nat. Mater.* **2012**, *11*, 963–969. [CrossRef]

16. Hwang, H.; Kim, H.; Cho, J. MoS(2) nanoplates consisting of disordered graphene-like layers for high rate lithium battery anode materials. *Nano Lett.* **2011**, *11*, 4826–4830. [CrossRef]

17. Zhang, A.; Li, A.; Zhao, W.; Liu, J. Recent Advances in Functional Polymer Decorated Two-Dimensional Transition-Metal Dichalcogenides Nanomaterials for Chemo-Photothermal Therapy. *Chemistry* **2018**, *24*, 4215–4227. [CrossRef]

18. Huang, Z.C.; Zhang, A.M.; Zhang, Q.; Pan, S.J.; Cui, D.X. Electrochemical Biosensor Based on Dewdrop-Like Platinum Nanoparticles-Decorated Silver Nanoflowers Nanocomposites for H_2O_2 and Glucose Detection. *J. Electrochem. Soc.* **2019**, *166*, B1138–B1145. [CrossRef]

19. Sangili, A.; Annalakshmi, M.C.; Chen, S.-M.; Balasubramanian, P.; Sundrarajan, M. Synthesis of silver nanoparticles decorated on core-shell structured tannic acid-coated iron oxide nanospheres for excellent electrochemical detection and efficient catalytic reduction of hazardous 4-nitrophenol. *Compos. Part B Eng.* **2019**, *162*, 33–42. [CrossRef]

20. Du, X.; Zhou, J. Application of biosensors to detection of epidemic diseases in animals. *Res. Vet. Sci.* **2018**, *118*, 444–448. [CrossRef]

21. Fani, M.; Rezayi, M.; Pourianfar, H.R.; Meshkat, Z.; Makvandi, M.; Gholami, M.; Rezaee, S.A. Rapid and label-free electrochemical DNA biosensor based on a facile one-step electrochemical synthesis of rGO-PPy-(L-Cys)-AuNPs nanocomposite for the HTLV-1 oligonucleotide detection. *Biotechnol. Appl. Bioc.* **2020**. [CrossRef] [PubMed]

22. Du, X.; Chen, Y.; Dong, W.H.; Han, B.K.; Liu, M.; Chen, Q.; Zhou, J. A nanocomposite-based electrochemical sensor for non-enzymatic detection of hydrogen peroxide. *Oncotarget* **2017**, *8*, 13039–13047. [CrossRef] [PubMed]

23. Bo, X.; Ndamanisha, J.C.; Bai, J.; Guo, L. Nonenzymatic amperometric sensor of hydrogen peroxide and glucose based on Pt nanoparticles/ordered mesoporous carbon nanocomposite. *Talanta* **2010**, *82*, 85–91. [CrossRef] [PubMed]

24. Khan, M.M.; Ansari, S.A.; Lee, J.; Cho, M.H. Novel Ag@TiO$_2$ nanocomposite synthesized by electrochemically active biofilm for nonenzymatic hydrogen peroxide sensor. *Mater. Sci. Eng. C Mater. Biol. Appl.* **2013**, *33*, 4692–4699. [CrossRef]

25. Fu, Y.; Dai, J.; Ge, Y.; Zhang, Y.; Ke, H.; Zhang, W. A Novel Non-Enzymatic Electrochemical Hydrogen Peroxide Sensor Based on a Metal-Organic Framework/Carbon Nanofiber Composite. *Molecules* **2018**, *23*, 2552. [CrossRef]

26. Lu, H.; Yu, S.; Fan, Y.; Yang, C.; Xu, D. Nonenzymatic hydrogen peroxide electrochemical sensor based on carbon-coated SnO2 supported Pt nanoparticles. *Colloids Surf. B Biointerfaces* **2013**, *101*, 106–110. [CrossRef]

27. Tang, N.; Zheng, J.; Sheng, Q.; Zhang, H.; Liu, R. A novel H2O2 sensor based on the enzymatically induced deposition of polyaniline at a horseradish peroxide/aligned single-wall carbon nanotubes modified Au electrode. *Analyst* **2011**, *136*, 781–786. [CrossRef]

28. Pei, Y.; Hu, M.; Tang, X.; Huang, W.; Li, Z.; Chen, S.; Xia, Y. Ultrafast one-pot anodic preparation of Co3O4/nanoporous gold composite electrode as an efficient nonenzymatic amperometric sensor for glucose and hydrogen peroxide. *Anal. Chim. Acta* **2019**, *1059*, 49–58. [CrossRef]

29. Guler, M.; Turkoglu, V.; Kivrak, A.; Karahan, F. A novel nonenzymatic hydrogen peroxide amperometric sensor based on Pd@CeO$_2$-NH$_2$ nanocomposites modified glassy carbon electrode. *Mater. Sci. Eng. C Mater. Biol. Appl.* **2018**, *90*, 454–460. [CrossRef]

30. Hussain, S. Comparative efficacy of epigallocatechin-3-gallate against H_2O_2-induced ROS in cervical cancer biopsies and HeLa cell lines. *Wspolczesna Onkol.* **2017**, *21*, 209–212. [CrossRef]